To appear in the *Journal of Geophysical Research*, 2000.

The leading variability mode of the coupled troposphere-stratosphere winter circulation in different climate regimes

Judith Perlwitz, Hans–F. Graf, and Reinhard Voss
Max–Planck Institute for Meteorology, Hamburg, Germany

Abstract

The leading variability mode of the coupled troposphere-stratosphere winter circulation in the Northern Hemisphere (NH) describes a close relationship between the strength of the stratospheric cyclonic vortex and the index of a tropospheric wave-like pattern covering the North Atlantic-Eurasian region. This mode can be determined by applying singular value decomposition analysis between the time series of winter mean NH 50- and 500-hPa geopotential heights. We compared the features of the leading coupled variability mode between two climate regimes, determined from a 1900-year integration with the coupled atmosphere-ocean climate model ECHAM3-LSG. The two regimes differ on the interdecadal timescale in the strength of the stratospheric polar vortex and therefore in the transmission-refraction properties of vertically propagating tropospheric waves. The spatial structures of the leading coupled variability mode of observational data better match the corresponding structures of the model's weak polar vortex regime (PVR) than those of the strong one. Because of the more effective tropospheric trapping of stationary wave energy of zonal wave number (ZWN) 2 at midlatitudes, the zonal variability structure of this wave is changed by barotropic effects in the troposphere as well as in the stratosphere. The coupled troposphere-stratosphere mode and the response of winter circulation were studied in a climate-change experiment carried out with the same model. We could show that under increased greenhouse gas forcing, both the response and the coupled variability mode between tropospheric and stratospheric circulation itself has a high similarity to the leading coupled mode in the strong PVR.

1. Introduction

During the cold season the stratosphere and troposphere are dynamically linked by wave-mean flow interaction [*Charney and Drazin,* 1961; *Matsuno,* 1970]. To isolate fundamental spatial structures characterizing this dynamical interaction, the quasi-stationary coupled variability modes between tropospheric and stratospheric winter circulation of the Northern Hemisphere (NH) were determined [*Baldwin et al.,* 1994; *Cheng and Dunkerton,* 1995; *Kodera et al.,* 1996; *Perlwitz and Graf,* 1995].

The leading variability mode of NH tropospheric and stratospheric winter circulation shows that the strength of the stratospheric polar vortex is closely related to an index of a well-defined teleconnection pattern of midtropospheric geopotential heights. If the stratospheric polar vortex is anomalously strong, the center of action over the Greenland-Davis Strait shows negative anomalies, while positive anomalies are observed in midlatitudes over the western Atlantic, western Europe, and eastern Asia. As a result, the tropospheric west wind over the North Atlantic is anomalously strong, corresponding to a positive index of the North Atlantic Oscillation (NAO). Tropospheric circulation anomalies of the opposite sign are found when the stratospheric polar vortex is anomalously weak. *Thompson and Wallace* [1998] showed that the Arctic Oscillation (AO), which has a center of action more over the Arctic than the NAO, is related to the variability of the strength of the stratospheric polar vortex. The leading coupled mode is also linked to pronounced regional anomalies in both lower tropospheric temperature and precipitation [*Thompson and Wallace,* 1998; *Koide and Kodera,* 1999; *Thompson and Wallace,* 1999; *Perlwitz and Graf,* 1995]. *Baldwin and Dunkerton* [1999] found that the 90-day low-pass-filtered anomalies of the AO, which is represented by the leading empirical orthogonal function (EOF) of variability of wintertime geopotential between 1000 and 10 hPa, typically appear first in the stratosphere and propagate downward to the surface within about 3 weeks. *Kitoh et al.* [1996] showed that the anomaly patterns of tropospheric circulation related to the variation of the strength of the stratospheric polar-night vortex are similar in observations and their climate model.

The positive phase of this leading coupled mode, corresponding to an anomalously strong polar-night vortex, can be exaggerated by stratospheric aerosol from tropical volcanic eruptions [*Kodera,* 1994; *Graf et al.,* 1993] and at the end of boreal winter by reduced ozone concentration in the lower stratosphere [*Graf et al.,* 1998]. Results from a global climate model including an interactive parameterization of stratospheric chemistry show that solar activity affects tropospheric climate because upper stratospheric ozone changes exaggerate the leading variability mode of the coupled troposphere-stratosphere circulation [*Shindell et al.,* 1999b].

There is an increasing body of evidence that not only interannual but also observed interdecadal variations of the winter circulation are manifested by this leading variability mode of atmospheric circulation [*Kodera and Koide,* 1997; *Thompson et al.,* 1999; *Graf et al.,* 1995,1998]. The observed 40-year cold season trend patterns of stratospheric circulation and both tropospheric circulation and temperature have a high similarity to the associated patterns corresponding to the positive phase of the leading coupled variability mode.

The main goal of this paper is to discuss the features of the leading coupled variability mode of winter mean troposphere-stratosphere circulation, as they appear on the interannual timescale, in two different climate regimes. The two regimes differ in the mean strength of the stratospheric polar vortex. A preferred excitation of a strong polar vortex by external forcing or internal variability of the coupled atmosphere-ocean climate system over several years may lead to a preferred trapping of planetary wave energy in the troposphere. This may change the structure of these coupled variability modes of atmospheric circulation determined with linear statistical methods. The observed records of tropospheric and stratospheric circulation (about 42 years) are too short for the investigation of variability modes in a strong polar vortex state. For the determination of coupled modes with multivariate statistical methods, a higher number of realizations is needed to gain reliable analysis results. Therefore we used the 1900-year control integration carried out with the coupled atmosphere-ocean general circulation model (AOGCM) ECHAM3-LSG, although its stratosphere is only marginally represented. *Feser et al.* [1999] showed that secular variability of the strength of the stratospheric polar-night vortex can be found in this integration. The knowledge about the spatial structures of the leading coupled mode in a strong polar vortex regime will be used for the understanding of features of both the coupled variability under increased anthropogenic greenhouse gas (GHG) forcing

and the structure of climate change response of the atmospheric circulation itself. For this study we used a climate change experiment, carried out with the same AOGCM.

The plan of this paper is as follows: Section 2 describes the used data and analysis method. Aspects of the structure and coupling between the troposphere and stratosphere in the control integration are discussed in section 3. The leading coupled atmospheric modes in the model's strong and weak polar vortex regimes are shown in section 4. In section 5 we discuss the exaggeration of the leading coupled mode by increased GHG concentration and the features of the coupled mode under increased anthropogenic forcing. The discussion and conclusions are given in section 6.

2. Data and Applied Analysis Method

We studied a long-term control integration of 1900 years and a GHG experiment forced with observed CO_2 concentrations from 1880 to 1985 and concentrations according to the Intergovernmental Panel on Climate Change (IPCC) scenario A (business as usual) [*Houghton et al.,* 1990] from 1986 to 2084. Both the control run and the experiment were carried out with the AOGCM ECHAM3-LSG. The atmospheric circulation model ECHAM3, a global low-order spectral model, is a version of the European Center operational weather forecast model with physical parameterizations modified for climate modeling purposes [*Roeckner et al.,* 1992]. The model was run with a triangular truncation at wave number 21 (T21), corresponding to a horizontal resolution of about 5.6°, and with 19 vertical levels between the Earth's surface and 10 hPa. The ocean model used was the large scale geostrophic model (LSG) based on primitive equations [*Maier-Reimer et al.,* 1993]. The coupled model and the first 500 years of the control run were described by *Voss et al.* [1998]. *Timmermann et al.* [1998] studied a coupled atmosphere-ocean mode, inherent in this model integration. The AOGCM ECHAM3-LSG has been used for climate change studies, sensitivity experiments, and detection studies [*Hasselmann et al.,* 1995; *Cubasch et al.,* 1997; *Hegerl et al.,* 1997]. The ECHAM3 model, coupled with a chemical module CHEM [*Steil et al.,* 1998], was used by *Dameris et al.* [1998] to estimate the future development of the ozone layer superposed on an increased GHG forcing.

We used National Centers for Environmental Prediction (NCEP) reanalysis data [*Kalnay et al.,* 1996] for the comparison between model and observational patterns. The similarity of the patterns is given by pattern correlation coefficients.

One objective of this paper is to compare different samples of the model integration in representing the simultaneous temporal variability of tropospheric and stratospheric circulation. Because we are interested in covariance structures, singular value decomposition (SVD) analysis is applied [*Cherry,* 1996]. The SVD analysis is a generalization of the EOF analysis. The latter method determines patterns (EOFs) describing maximum variance in a single field, whereas SVD analysis selects the patterns (singular patterns) which describe maximum covariance between two fields. This multivariate method was highly recommended by *Bretherton et al.* [1992] and *Wallace et al.* [1992] for isolating coupled modes of variability between the time series of two geophysical fields. Since the publication of these two papers, the SVD analysis has become a common method in climate research. SVD analysis seems to be predestined for a comparison of preferred coupled modes because the statistical results are easy to interpret and require no user-supplied parameters [*Bretherton et al.,* 1992]. Precautions for avoiding the occurrence of spurious correlated patterns between two fields using this method were stressed by *Newman and Sardeshmukh* [1995]. This risk is increased if the sample size is small [*Bretherton et al.,* 1992; *Cherry,* 1996]. However, the same problem also exists when using other statistical techniques.

We applied SVD analysis between the NH (north of 20°N) 50- and 500-hPa geopotential heights on the basis of winter means (December to February). The time series at the grid points were weighted with the square root of the cosine of the geographical latitude. Thus our analysis agrees with the approach of *Baldwin et al.* [1994]. They determined the leading coupled mode on the basis of winter mean observations using SVD analysis. We show homogeneous and heterogeneous regression and correlation patterns as described by *Bretherton et al.* [1992] and *Cheng and Dunkerton* [1995]. The maps of regression coefficients shown correspond to one standard deviation (σ) of the temporal expansion coefficients of the SVD singular patterns.

We have stated that the leading coupled mode of stratospheric and tropospheric circulation depicts a relationship between the strength of the stratospheric cyclonic vortex and the index of a tropospheric wave-like pattern and that this mode evolves

from the interaction between tropospheric ultralong planetary waves and the mean stratospheric flow. Thus the leading coupled mode between tropospheric and stratospheric winter circulation reflects not only a mathematical filtering (by maximizing the covariance) but also a dynamical one, and the hemispheric variability modes of atmospheric circulation are isolated in context of a specific physical process.

3. Stratospheric Features of the Leading Coupled Mode in the ECHAM3-LSG Model

The leading coupled variability mode between the time series of NH 50- and 500-hPa geopotential heights in the 1900-year integration of the ECHAM3-LSG model captured the main relationship found in observational data [e.g., *Baldwin et al.,* 1994]. The coupled variability mode describes the connection between the strength of the stratospheric polar vortex and a tropospheric circulation pattern characterized by a hemispheric pressure seesaw between high and middle latitudes, whereas the closest relationship can be found over the North Atlantic region. The fraction of explained total squared covariance of the first (leading) mode is less in the model (60%) than in observational data (76%) determined on the basis of observed 41 winter means. Nevertheless, the model's leading mode is well separated from the second mode, explaining 22% of total squared covariance. The correlation between the expansion coefficients of the singular patterns (not shown) is 0.66.

There are some notable differences between observations and the climate model in the spatial structure of this mode. In this section we want to focus on the stratospheric part of the coupled circulation mode. Figure 1 shows the 50-hPa geopotential height field regressed onto the time series of the expansion coefficients of the 50-hPa singular pattern. The variability center of the stratospheric polar vortex is displaced toward the Pacific in the model, whereas it is stronger over the North Atlantic in observational data. The interannual variability of the model's stratospheric polar-night vortex, as depicted in this coupled mode, is remarkably less than in observations. Over the North Pole the variability corresponding to one standard deviation of the index time series of the stratospheric field is, with approximately 120 geopotential meters (gpm), only almost half as large as observed (210 gpm). One reason is an overly strong polar-night vortex, which is a common bias in most climate models with an upper boundary set already at 10 hPa. This reduces the possibility of disturbances of the stratospheric circulation by tropospheric planetary waves [*Boville and Cheng,* 1988] and therefore the variability in the strength of the stratospheric polar vortex. As a result, at the 50-hPa pressure level, the long-term winter mean temperature at the North Pole amounts to $-78°$C, which is 9 K colder than observed ($-69°$C), and the long-time mean west wind at 60°N is 9 m/s stronger than observed. Another cause for the reduced variability of the strength of the stratospheric polar vortex in the model results from the absence of external forcing (e.g., volcanic eruptions and solar activity) and of the quasi-biennial oscillation (QBO) in the tropical stratosphere. The phase of the QBO, through modulation of the zonal mean zonal wind, affects the upward and equatorward propagation of ultralong planetary waves [*Dunkerton and Baldwin,* 1991].

We studied the differences in the meridional and vertical propagation of stationary waves between the two states of the leading coupled mode (anomalously weak and strong polar vortex) in the control integration of the climate model. As a diagnostic tool, the Eliassen-Palm flux (E-P flux) is used, which indicates the wave activity and energy propagation. We selected the composites of the E-P flux for the two states on the basis of temporal expansion coefficients of the 50-hPa pattern of the leading mode. From the 1899 individual winter means, 305 years were characterized by an anomalously strong polar vortex ($\sigma > 1$). The composite for an anomalously weak stratospheric vortex ($\sigma < -1$) is calculated from 289 years.

The meridional cross section of the difference vector of the E-P flux composites (not shown) exhibits the known features of energy flux when the influence of the strength of stratospheric polar vortex is studied [*Boville,* 1984; *Kodera and Koide,* 1997]. When the polar vortex is anomalously strong, the vertical propagation of stationary wave energy in the stratosphere and the northward flux within the troposphere are significantly reduced, indicating an anomalously strong trapping of stationary wave energy in the troposphere. We also determined composites of the E-P flux for the individual stationary zonal waves by expanding the geopotential height fields in their zonal Fourier harmonics. The contribution of the individual waves to the total E-P flux is additive and depends on the square of the amplitude and the latitudinal and vertical derivatives of the phase of the individual waves [*Andrews et al.,* 1987]. Figure 2 shows

the meridional cross section of the difference vectors (strong minus weak polar vortex) for the zonal wave numbers (ZWNs) 1 and 2. When the polar vortex is anomalously strong, the vertical propagation of wave energy of ZWN 1 in the stratosphere is reduced between 60° and 85°N but increased between 40° and 50°N, and an increased southward propagation in the midtroposphere can be found. Thus planetary wave energy of ZWN 1 is more effectively trapped in the troposphere at high latitudes in the strong polar vortex state than in the weak one. At midlatitudes (between 40° and 60°N), a more effective trapping of stationary wave energy of ZWN 2 in a strong polar vortex state dominates. A reduced vertical propagation of ZWN 2 into the stratosphere and a reduced northward propagation in the midtroposphere can be found. As a consequence of the reduced propagation of wave energy into the stratosphere by waves of ZWN 1 and 2, the North Pole temperature at the 50-hPa level is significantly lower (−81°C) than in the weak polar vortex case (−76°C). The discussed results are significant at least at the 95% level.

4. The Leading Coupled Mode in the Strong and Weak Polar Vortex Regime

4.1. The Definition of the Strong and Weak Polar Vortex Regime

The preferred exaggeration of a strong polar-night vortex in a particular analysis period may change the structure of linear variability modes in the atmospheric circulation because the waves are trapped more effectively in the troposphere. We used the studied long-term integration of AOGCM ECHAM3-LSG to compare the leading coupled mode on the interannual timescale in a strong and weak polar vortex state. *Feser et al.* [1999] studied the interannual variability of winter mean NH zonal mean zonal wind in the long-term integration of the ECHAM3-LSG model and found considerable variations on the secular timescale. Following the linear theory, the vertical propagation of planetary waves into the stratosphere depends on a critical velocity which decreases with an increasing zonal wave number [*Charney and Drazin,* 1961]. Thus linear changes in the strength of the stratospheric polar vortex can be connected with nonlinear effects in tropospheric circulation because a critical velocity for a specific wave is involved. We took into consideration this threshold problem for the selection of periods which are characterized by a preferred exaggeration of a strong or weak polar vortex in the control run. We counted how often the expansion coefficient of the singular pattern of the 50-hPa field is larger (smaller) than σ ($-\sigma$) during a 30-year period, where σ is the long-term standard deviation of the temporal expansion coefficients. In the following, $N_{>\sigma}$ and $N_{<-\sigma}$ stand for the number of positive and negative enhancements, respectively. In section 3 we have shown that the characteristics of vertical propagation for waves of ZWN 1 and 2 are different between both states. We used the ratio $rat_{30} = N_{>\sigma}/N_{<-\sigma}$ as a measure which indicates the preference of the positive enhancement ($rat_{30} > 1$, anomalously strong polar vortex) or the negative enhancement ($0 < rat_{30} < 1$, anomalously weak polar vortex) of the regression pattern (Figure 1) within the studied 30-year period. To avoid $N_{<-\sigma}$ becoming zero, both $N_{<-\sigma}$ and $N_{<\sigma}$ were set equal to 1 before counting. Figure 3 shows the time series of this ratio at the 50-hPa level, determined for overlapping 30-year periods. This smoothed time series does not emphasize single extreme anomalies as does a 30-year running average.

The visual inspection of this time series shows a pronounced secular variability, characterized by periods in which an anomalously strong vortex is more often excited than an anomalously weak one or vice versa. The respective periods which clearly differ in the preference of a strong and weak stratospheric vortex are called strong and weak polar vortex regimes (PVR).

4.2. The Leading Coupled Mode in the Strong and Weak PVR

To study the interannual coupled variability between tropospheric and stratospheric winter circulation in the climate model within the two PVRs, we selected periods permanently characterized by a ratio rat_{30} larger (smaller) than one standard deviation [$\sigma_{log(rat_{30})} = 0.23$]. The composed time series for the strong (weak) PVR consist of a total of 174 (194) years. We applied the SVD analysis between the 50- and 500-hPa geopotential height fields for the composed data set of the strong and weak PVR, separately. As expected, the total covariance between the NH 50- and 500-hPa geopotential fields is higher in the weak than in the strong PVR. The extra covariance in the weak PVR is mainly concentrated in the first SVD mode, explaining 61% of total squared covariance, whereas the fraction amounts to 52% in the strong PVR.

Figure 4 compares the associated (heterogeneous) regression patterns of the strong and weak PVR. The shading represents the heterogeneous correlation patterns. The light and dark shadings indicate "remarkable" absolute correlation coefficients larger than 0.3 and 0.5, respectively (a correlation coefficient of 0.2 is already significant at the 95% level). The pattern correlation between the regression patterns of the observations and a model regime indicate that the weak PVR of the model better matches the observed mode than the model's strong PVR. The agreement of the 500-hPa patterns between observations and the weak (strong) PVR further increases (decreases) when the spatial structures north of 35°N (instead of 20°N) are compared. The 50-hPa pattern of the weak PVR (Figure 4a) clearly shows a pronounced circumpolar pressure seesaw, whereas the corresponding pattern of the strong PVR (Figure 4b) depicts a more zonally asymmetric structure. This becomes clear from Table 1, which contains the zonal mean geostrophic wind and the amplitudes of both ZWNs 1 and 2 at 58°N of the 50- and 500-hPa regression patterns shown in Figure 4. This latitude is representative for the latitude belt between 50° and 70°N. In comparison with the weak PVR, the meridional gradient of the regression pattern of the 50-hPa field in the strong PVR, and thus the zonal mean geostrophic wind, is reduced, whereas the amplitude of the waves of both ZWN 1 and 2 is visibly increased. Table 1 also indicates that the difference in the heterogeneous regression patterns of the 500-hPa geopotential heights between both regimes mainly results from a higher amplitude of the ZWN 2 component in midlatitudes in the strong PVR. At the same time, the variability of waves of ZWN 1 is reduced in the pattern of the strong PVR between 35° and 45°N. At 42°N the reduction amounts to about 4 gpm. As a result of these differences in the zonal wave structure of the coupled variability patterns, the node line between positive and negative anomalies over both the North Atlantic and the North Pacific is shifted southward in the strong PVR relative to the weak one. Over the North Atlantic this shift is quite small (about 5°), but over the North Pacific it amounts to about 20°.

During winter, owing to advective processes, circulation anomalies are closely related to lower tropospheric temperature anomalies. The 850-hPa temperatures regressed onto temporal expansion coefficients of the 50-hPa singular pattern are given in Figure 5. Again, the regression pattern of the weak PVR better matches the observations [*Koide and Kodera,* 1999; *Perlwitz and Graf,* 1995] than the pattern of the strong PVR, which exhibits a pronounced cold-ocean-warm-land variation between 50° and 80°N.

Comparing the regression patterns of the 500-hPa field between the model's weak PVR (Figure 4c) and observations, a difference in the positions of the positive and negative centers of the 500-hPa pressure anomalies over the North Atlantic can be found. In observations, an anomalously strong vortex is connected with a stronger than normal southwesterly wind over the eastern North Atlantic, causing an intensified advection of mild and wet maritime air to northwest Europe [*Koide and Kodera,* 1999; *Perlwitz and Graf,* 1995]. In the model's weak PVR the North Atlantic centers of action, as depicted in the tropospheric regression pattern of the leading coupled mode, are arranged meridionally, and their node line is mainly zonally directed. Therefore, in connection with this coupled circulation mode in the climate model, this advective influence of the circulation on the temperature of northwest Europe is underestimated.

A still-to-strong polar vortex in the weak PVR, and a relatively low spatial resolution (T21) smoothing the orography in the model, may explain the structural differences between the observed and the modeled tropospheric pattern. However, we found a visible reduction in the structural bias of the leading atmospheric circulation mode in the weak PVR in comparison with the total model integration, although the reduction of the cold bias in the high-latitude 50-hPa temperature amounts to only 1 K.

4.3. Causes of the Structural Differences Between the Coupled Modes of Both Regimes

We studied in more detail whether the strong differences in the leading atmospheric variability mode can be mainly attributed to the preferred enhancement of an anomalously strong polar-night vortex. From the results of the SVD analyses, it cannot be concluded that the circulation in the strong PVR is characterized by a higher variability of midlatitude waves of ZWN 2. We compared the standard deviation of the amplitude of this stationary wave, determined from the geopotential height fields, between both PVRs and did not find any significant differences. Another possibility is that in the strong PVR the variability of waves of ZWN 2 is more stationary than in the weak PVR. This would be an indication of the stronger effect of the tropospheric trapping of wave energy in the strong PVR, which is

connected with an increase of equivalent-barotropic effects [*Boville and Cheng,* 1988]. To study the spatial variability structure of the individual zonal waves, EOF analysis was used. We selected a specific latitude and expanded the individual realizations of the geopotential height fields in their zonal Fourier harmonics. Let z_k be anomalous geopotential height fields related to the kth zonal wave component at a specific latitude. Then z_k at the longitude λ of the year t is expressed as follows:

$$z_k(\lambda, t) = a(t)\cos(k\lambda) + b(t)\sin(k\lambda).$$

If the longitudinal structure of the year-to-year variation is geographically fixed, the time series $a(t)$ and $b(t)$ are not independent. One EOF can, then, explain the total variability of the latitudinal field z_k. Contrary to this, when this variation is randomly distributed, the correlation between $a(t)$ and $b(t)$ becomes zero and the total variance is equally shaded by two EOFs (50% each). Therefore the fraction of variance explained by the leading EOF can be used as a measure of the stationarity of the variation of the wave of ZWN k at a specific latitude.

We performed this analysis for the waves of both ZWN 1 and 2, at each latitude of the NH (north of 20°N) grid and each available pressure level between 1000 and 30 hPa. The explained fractions of total variance of the leading EOF, obtained from the individual analyses, are combined as a meridional cross section. Figures 6a and 6c show these meridional cross sections of ZWN 1 and 2, respectively, for the weak PVR. The meridional cross section of the difference of this parameter between the strong and weak PVR (strong minus weak) is given in Figures 6b (ZWN 1) and 6d (ZWN 2). In the weak PVR a strong stationarity of waves of ZWN 1 can be found in the troposphere around 25°N and between 40° and 50°N. At midlatitudes more than 75% of total variance is explained by the leading EOF from the surface to the 150-hPa level. In the strong PVR the tropospheric centers of stationarity are shifted southward and are slightly increased. In the weak PVR the two tropospheric centers of high stationarity for ZWN 2 can be found around 30°N and between 55° and 65°N. In the strong PVR the degree of stationarity is more than 10% higher in both centers. For the midlatitude center the difference increases with increasing altitude, and the leading EOF of ZWN 2 explains more than 70% of total variance from the surface to the 50-hPa level. At these latitudes the highest amplitude of the leading EOF can be found. We also determined the phase of the first EOF of ZWN 2, for example, the longitude where the first extremum (minimum or maximum) of the wave is found. At midlatitudes, where the maximum change in the degree of stationarity occurs in the upper troposphere and lower stratosphere, we found an eastward shift of phase in the strong PVR relative to the weak one. For instance, at 58°N and the 500-hPa level the phase amounts to 63°E and 72°E for the weak and strong PVR, respectively. The eastward phase shift decreases with increasing height. This shift amounts to 5° and 2° at the 200-hPa and 50-hPa level, respectively. At higher altitudes the increase of stationarity of the variability of ZWN 2 is more important.

As expected in a strong PVR, the dynamical coupling between the troposphere and stratosphere is considerably reduced. We have shown that this is related to a change in the spatial structure of the leading coupled variability mode of tropospheric and stratospheric circulation in the studied climate model. In the strong PVR the more effective tropospheric trapping of stationary wave energy of ZWN 2 at midlatitudes changes the zonal variability structure of this stationary wave in the troposphere as well as in the stratosphere. In the next section we want to give an application of the knowledge about the spatial structure of the associated patterns in a strong PVR.

5. The Exaggeration of the Leading Coupled Mode by the Increased Greenhouse Effect

Palmer [1993] suggested that the impact of enhanced atmospheric CO_2 concentration manifests itself as an increase in certain preferred patterns of internal variability of the atmosphere rather than in some new pattern of atmospheric variability which is orthogonal to the internal modes. Orthogonality of the response pattern is the main prerequisite for the application of optimal fingerprint analysis [*Hasselmann,* 1993]. There is a physical process which can explain the exaggeration of the leading coupled variability mode by increasing GHG forcing via changes in the stratospheric circulation [*Perlwitz and Graf,* 1995]. The increase in tropospheric temperature and humidity in lower latitudes due to the combined greenhouse effect leads to a lifting of the lower-latitude geopotential height layers and thus to an initial intensification of the polar-night vortex by the strengthening of the thermal wind. The climate change sensitivity experiments of *Shindell et al.*

[1999a] and *Graf et al.* [1995] show a strengthening of the stratospheric polar vortex with rising anthropogenic forcing. An intensified polar vortex is related to changed transmission-refraction properties of vertically propagating tropospheric waves and may produce tropospheric circulation anomalies similar to the positive phase of the leading coupled circulation mode.

Therefore we studied the exaggeration of the coupled mode of atmospheric winter circulation due to anthropogenic GHG forcing in an experiment, carried out with the ECHAM3-LSG model. The GHG forcing is based on observations (1880-1985) and the IPCC (1990) scenario A (business as usual, 1986-2084) [*Houghton et al.,* 1990]. The yearly winter (December-January-February) response patterns were calculated as difference patterns between the individual winter means of the GHG experiment and the long-term winter mean of the control run. The global average was removed from the individual winter mean geopotential height fields of the scenario simulation before determining the difference patterns. This allows one to neglect the global mean increase in the geopotential height caused by the thermal expansion of the atmosphere due to increasing temperature. We projected these difference patterns of 50- and 500-hPa geopotential heights onto the respective singular patterns, isolated by SVD analysis of the total unforced model run. The time series of the projections, normalized by the standard deviation of the respective control run, σ_C, are shown in Figure 7. After 1980 a preferred enhancement of the positive phase of the main coupled circulation mode, both in the stratosphere and in the troposphere, can be seen. The interannual variability, as it is depicted in this coupled mode, decreases with the increase of the GHG concentration. Extremes only occur in the positive phase of this mode.

The time series for 50-hPa geopotential heights (Figure 7a) reveals that in the studied GHG forcing experiment, the stratospheric polar vortex strengthens continuously with increasing GHG concentration. This changes the condition for the vertical propagation of tropospheric planetary waves. Thus a reduction of dynamical interaction between tropospheric and stratospheric circulation under stronger GHG forcing may be connected with a transition to a new dynamic regime similar to the strong PVR which was isolated in the control run. To isolate the leading coupled variability mode of stratospheric and tropospheric circulation under stronger GHG forcing, we performed a SVD analysis between winter mean NH 50- and 500-hPa geopotential heights using the last 70 years of the GHG simulation (2014-2084). The long-term local trends were removed before applying the SVD approach. As expected, the associated patterns capture very well the features of the corresponding patterns of the strong PVR. We found that the concurrent variation of the meridional pressure seesaw over the North Atlantic and North Pacific of NH 500-hPa circulation (Figure 8) is more pronounced than in the model's strong PVR (Figure 4d). Both high-latitude centers of action over the ocean show about the same value of the regression coefficient (25 gpm), whereas the meridional pressure seesaw in the strong PVR is clearly stronger over the North Atlantic than over the North Pacific. In the studied climate change experiment the strength of the seesaw over the North Atlantic is visibly reduced under increased anthropogenic forcing. Relative to the regression map of the strong PVR of the control run, the map of the GHG experiment shows a southward shift of the node line between positive and negative anomalies over both oceans. Additionally, an eastward shift of the centers of action over the North Atlantic is found. The latter result corresponds partly to the study of *Ulbrich and Christoph* [1999]. They studied the shift of the centers of action of the NAO with increasing GHG forcing in the AOGCM ECHAM3/OPYC (T42), using sea level pressure, and found a northeastward shift.

We were also interested in the consequences of a polar vortex intensified by increased GHG concentration for the structure of the response in atmospheric circulation. With the associated patterns of the leading coupled mode in the different PVRs, a basis for such an analysis is given. We studied the similarity between the climate change response in tropospheric and stratospheric circulation and the associated patterns of the coupled troposphere-stratosphere circulation in the weak and strong PVR. We determined spatial pattern correlations between the patterns of the model response of NH 50- and 500-hPa geopotential heights with the singular patterns of the coupled modes for both the strong and weak PVR. This correlation coefficient can vary between -1.0 and 1.0 and clearly stresses the structural pattern similarity and not the anomalies. The time series of pattern correlation determined for overlapping decadal mean (11-year) response patterns are given in Figure 9. The overlapping decadal averages reduce the spatial and temporal noise associated with higher-frequency variability. After 1990, there is, in general, a higher sim-

ilarity between the response patterns and the associated patterns of the model's strong PVR than of the weak one. For the strong PVR the pattern correlations of the 50-hPa level fluctuate between 0.6 and 0.7, while the spatial pattern correlations of the 500-hPa level are higher and can reach values greater than 0.8, explaining about 70% of the 11-year smoothed spatial response structure.

We also studied the similarity between the response of the 850-hPa temperature and the regression patterns shown in Figure 5. The temporal course (Figure 9c) follows mainly the time series of spatial pattern correlation of the 500-hPa geopotential height field. The mean pattern correlation coefficients after 1990 amount to about 0.6 for the pattern of the strong PVR, indicating that 36% of the hemispheric response can be explained.

We have shown that the strength of the stratospheric polar vortex is a control parameter for the structure of the climate change response in tropospheric temperature and circulation in the studied climate change experiment. The spatial pattern correlation remains smaller than 1.0 because other processes, the air-sea interaction, for example, are also very important for the development of the climate change response [*Timmermann et al.,* 1998, 1999].

6. Discussion and Conclusions

We studied the leading coupled mode between the time series of NH 50- and 500-hPa geopotential heights for two climate regimes of a 1900-year control run, carried out with the AOGCM ECHAM3-LSG (T21). The two regimes differ on the interdecadal timescale in the strength of the stratospheric polar vortex and therefore in the transmission-refraction properties of vertically propagating tropospheric waves. We found that this difference has consequences for the spatial structures of the coupled mode between both regimes, which were determined with a linear statistical analysis method. The spatial structures of the leading coupled variability mode of observational data better match the corresponding patterns of the model's weak PVR than those of the strong one's. In the model's strong PVR the concurrent variation of waves of ZWN2 in the troposphere and stratosphere is increased, whereas the interaction of tropospheric waves with the mean stratospheric flow is reduced. Because of the more effective tropospheric trapping of stationary wave energy of ZWN2 at midlatitudes, the zonal variability structure of this wave on the interannual timescale is considerably influenced by barotropic effects in the troposphere as well as in the stratosphere. For the studied integration with the AOGCM ECHAM3-LSG, we could show that the phase in which the North Atlantic and the North Pacific varies concurrently on the interannual timescale is influenced by the strength of the stratospheric polar vortex during the analysis period. During periods with a preferred exaggeration of a strong polar vortex, the inphase variation of both atmospheric regions is emphasized. Our analysis is clearly focused on the investigation of atmospheric circulation modes. On the interannual timescale, the variability of the sea surface temperature is primarily forced by atmospheric variability [e.g., *Delworth,* 1996]. For the explanation of atmospheric variability on multiyear to multidecadal timescales, however, the interaction of the atmosphere with the ocean becomes important [e.g., *Rodwell et al.,* 1999]. With this paper we wanted to show that besides the ocean, the strength of the stratospheric polar vortex is also an important parameter for the understanding of both variability modes of the atmosphere-ocean system of a climate model [e.g., *Timmermann et al.,* 1998] and features of observed climate variability. Further studies are required to determine whether a changed tropospheric anomaly structure, resulting from changes in the strength of the stratospheric polar vortex in individual years, contributes to the amplification and stabilization of longer timescale modes of the atmosphere-ocean system.

The leading coupled variability mode of the troposphere-stratosphere circulation as well as the response of winter circulation were studied in a climate change experiment with increasing GHG concentration carried out with the same model. In this experiment a large part of the climate change signal is carried by the leading coupled mode. This result confirms the idea of *Palmer* [1993] that the impact of enhanced atmospheric GHG concentration manifests itself mainly as an increase in certain preferred patterns of internal variability of the atmosphere. We clearly focused on the winter season and isolated physically filtered patterns representing the related variation of stratospheric and tropospheric circulation on the interannual timescale. We could show, however, that the spatial structure of the climate change patterns alters with increased forcing. One parameter for this change is the intensification of the stratospheric polar vortex with increasing greenhouse effect. This in-

tensification leads not only to an exaggeration of the positive phase of the leading coupled variability mode but also to a change in the structure of this mode. Under increased GHG forcing, both the response and the coupled variability between tropospheric and stratospheric circulation itself have a high similarity to the leading coupled mode of the model's strong PVR. The changed structure of the leading coupled mode can be interpreted as the orthogonal signal evolving from external forcing that is studied in optimal fingerprint analysis [*Hasselmann,* 1993].

There are increasing efforts to attribute the cold-season climate change, which has been observed during the last 40 years, to the increased GHG effect. Our results emphasize two important points which have to be considered when comparing observed climate changes with the cold-season GHG response of sensitivity experiments with comprehensive climate models.

First, the strength of the stratospheric polar vortex of a climate model used for the study of climate changes during winter is one crucial parameter that determines the spatial structure of the climate response and the strength of the signal. This conclusion agrees with the results of *Shindell et al.* [1999a]. They found considerable differences in the change of the AO index, depending on the representation of the stratosphere in their climate model, which were forced with increasing GHG concentration.

Second, the representation of the variability of the planetary waves in the climate model influences the spatial structure of the winter responses in circulation and temperature. One reason is the intensification of the stratospheric polar vortex with rising GHG concentration, which leads to a change of the structure of planetary waves that are trapped in the troposphere when the polar vortex is intensified. The predominant change in the zonal structure of the variability of waves of ZWN2 may be partly attributed to the relatively coarse horizontal resolution (5.6°). Other important factors may be the vertical resolution and, as explained in the previous point, the top height of the model.

Thus an evaluation of climate models used for sensitivity experiments should include the investigation of the coupled variability modes of troposphere-stratosphere circulation. It is of the greatest importance that climate models properly represent the energy and structure of the leading atmospheric variability mode because this mode can be exaggerated by stratospheric aerosols from tropical volcanic eruptions [*Graf et al.,* 1993; *Kodera,* 1994], reduced ozone concentration at the end of the winter [*Graf et al.,* 1998], solar activity [*Shindell et al.*, 1999b], and, as demonstrated by *Shindell et al.* [1999a], *Graf et al.* [1995], and this study, the increasing anthropogenic greenhouse effect.

Acknowledgments. We thank the unknown reviewers for their very helpful comments on this manuscript. This work was supported by the Bundesministerium für Bildung, Wissenschaft, Forschung und Technologie (BMBF, Germany), grant 01 LO9512/0 (Ozone Research Program).

References

Andrews, D. G., J. Holton, and C. B. Leovy, *Middle Atmosphere Dynamics,* 489 pp., Academic Press, San Diego, Calif., 1987.

Baldwin, M. P., and T. J. Dunkerton, Propagation of the Arctic Oscillation from the stratosphere to the troposphere, *J. Geophys. Res.,* in press, 1999.

Baldwin, M. P., X. Cheng, and T. J. Dunkerton, Observed correlations between winter-mean tropospheric and stratospheric circulation anomalies, *Geophys. Res. Lett., 21,* 1141-1144, 1994.

Boville, B. A., Influence of the polar night jet on the tropospheric circulation in a GCM, *J. Atmos. Sci., 41,* 1132-1142, 1984.

Boville, B. A., and X. Cheng, Upper boundary effect in a general circulation model, *J. Atmos. Sci., 45,* 2591-2606, 1988.

Bretherton, C. S., C. Smith, and J. M. Wallace, An intercomparision of methods for finding coupled patterns in climate data, *J. Clim., 5,* 541-560, 1992.

Charney, J. G., and P. G. Drazin, Propagation of planetary-scale disturbances from the lower into the upper atmosphere, *J. Geophys. Res., 66,* 83-109, 1961.

Cheng, X., and T. J. Dunkerton, Orthogonal rotation of spatial patterns derived from singular value composition analysis, *J. Clim., 9,* 2631-2643, 1995.

Cherry, S., Singular value decomposition analysis and canonical correlation analysis, *J. Clim., 9,* 2003-2009, 1996.

Cubasch, U., R. Voss, G. C. Hegerl, J. Waszkewitz, and T. J. Crowley, Simulation of the influence of solar radiation variations on the global climate with an ocean-atmosphere general circulation model, *Clim. Dyn., 13,* 757-767, 1997.

Dameris, M., V. Grewe, R. Hein, C. Schnadt, C. Brühl, and B. Steil, Assessment of the future de-

velopment of the ozone layer, *Geophys. Res. Lett., 25,* 3579-3582, 1998.

Delworth, T. L., North Atlantic interannual variability in a coupled ocean-atmosphere model, *J. Clim., 9,* 2356-2375, 1996.

Dunkerton, T. J., and M. P. Baldwin, Quasi-biennial modulation of planetary-wave fluxes in the Northern Hemisphere winter, *J. Atmos. Sci., 48,* 1043-1061, 1991.

Feser, F., H.-F. Graf, and J. Perlwitz, Secular variability of the coupled tropospheric and stratospheric circulation in the GCM ECHAM3/LSG, *J. Theoret. Appl. Meteorol.*, in press, 1999.

Graf, H.-F., I. Kirchner, A. Robock, and I. Schult, Pinatubo eruption winter climate effects: Model versus observations, *Clim. Dyn., 9,* 81-93, 1993.

Graf, H.-F., J. Perlwitz, I. Kirchner, and I. Schult, Recent northern winter climate trends, ozone changes and increased greenhouse gas forcing, *Contrib. Atmos. Phys., 68,* 233-248, 1995.

Graf, H.-F., I. Kirchner, and J. Perlwitz, Changing lower stratospheric circulation: The role of ozone and greenhouse gases, *J. Geophys. Res., 103,* 11,251-11,261, 1998.

Hasselmann, K., Optimal fingerprints for the detection of time-dependent climate change, *J. Clim., 6,* 1957-1971, 1993.

Hasselmann, K., L. Bengtsson, U. Cubasch, G. C. Hegerl, H. Rodhe, E. Roeckner, H. von Storch, R. Voss, and J. Waszkewitz, Detection of anthropogenic climate change using a fingerprint method, in *Proceedings of Modern Dynamical Meteorology, Symposion in Honor of Aksel Wiin Nicelson,* edited by P. Dittevson, pp. 203-221, Eur. Cent. for Medium-Range Weather Forecasts, Reading, England, 1995.

Hegerl, G. C., K. Hasselmann, U. Cubasch, J. F. B. Mitchell, E. Roeckner, R. Voss, and J. Waszkewitz, Multi-fingerprint detection and attribution analysis of greenhouse gas, greenhouse gas-plus-aerosol and solar forced climate change, *Clim. Dyn., 13,* 613-634, 1997.

Houghton, J. T., G. J. Jenkins, and J. J. Ephraums (Eds.), *Climate Change: The IPCC Scientific Assessment,* Cambridge Univ. Press, New York, 1990.

Kalnay, E., et al., The NCEP/NCAR 40-Year Reanalysis Project, *Bull. Am. Meteorol. Soc., 77,* 437-471, 1996.

Kitoh, A., H. Koide, K. Kodera, S. Yukimoto, and A. Noda, Interannual variability in the stratospheric-tropospheric circulation in a coupled ocean-atmosphere GCM, *Geophys. Res. Lett., 23,* 543-546, 1996.

Kodera, K., Influence of volcanic eruptions on the troposphere through stratospheric dynamical processes in the Northern Hemisphere winter, *J. Geophys. Res., 99,* 1273-1282, 1994.

Kodera, K., and H. Koide, Spatial and seasonal characteristics of recent decadal trends in the Northern Hemispheric troposphere and stratosphere, *J. Geophys. Res., 102,* 19, 433-19,447, 1997.

Kodera, K., M. Chiba, H. Koide, A. Kitoh, and Y. Nikaidou, Interannual variability of the winter stratosphere and troposphere in the Northern Hemisphere, *J. Meteorol. Soc. Jpn., 74,* 365-382, 1996.

Koide, H., and K. Kodera, A SVD analysis between the winter NH 500-hPa height and surface temperature fields, *J. Meteorol. Soc. Jpn., 77,* 47-61, 1999.

Maier-Reimer, E., U. Mikolajewicz, and K. Hasselmann, Mean circulation of the Hamburg LSG OGCM and its sensitivity to the thermohaline surface forcing, *J. Phys. Oceanogr., 23,* 731-757, 1993.

Matsuno, T., Vertical propagation of stationary planetary waves in the winter Northern Hemisphere, *J. Atmos. Sci., 27,* 871-883, 1970.

Newman, M., and P. D. Sardeshmukh, A caveat concerning singular value decomposition, *J. Clim., 8,* 352-360, 1995.

Palmer, T. N., A nonlinear dynamical perspective on climate change, *Weather, 48,* 314-326, 1993.

Perlwitz, J., and H.-F. Graf, The statistical connection between tropospheric and stratospheric circulation of the Northern Hemisphere in winter, *J. Clim., 8,* 2281-2295, 1995.

Rodwell, M. J., D. P. Rowell, and C. K. Folland, Oceanic forcing of the wintertime North Atlantic Oscillation and European climate, *Nature, 398,* 320-323, 1999.

Roeckner, E., et al., Simulation of the present-day climate with the ECHAM model: Impact of model physics and resolution, *MPI-Rep. 93,* 169 pp., Max-Planck-Inst. für Meteorol., Hamburg, Germany, 1992.

Shindell, D. T., R. L. Miller, G. A. Schmidt, and L. Pandolfo, Simulation of recent northern winter climate trends by greenhouse-gas forcing, *Nature, 399,* 452-455, 1999a.

Shindell, D. T., D. Rind, N. Balachandran, J. Lean, and P. Lonergan, Solar cycle variability, ozone, and

climate, *Science, 284,* 305-308, 1999b.

Steil, B., M. Dameris, C. Brühl, P. J. Crutzen, V. Grewe, M. Ponater, and R. Sausen, Development of a chemistry module for GCMs: First results of a multiannual integration, *Ann. Geophys., 16,* 205-228, 1998.

Thompson, D. W. J., and J. M. Wallace, The Arctic Oscillation signature in the wintertime geopotential height and temperature fields, *Geophys. Res. Lett., 25,* 1297-1300, 1998.

Thompson, D. W. J., and J. M. Wallace, Annular modes in the extratropical circulation, part I: Month-to-month variability, *J. Clim.,* in press, 1999.

Thompson, D. W. J., J. M. Wallace, and G. C. Hegerl, Annular modes in the extratropical circulation, part II: Trends, *J. Clim.,* in press, 1999.

Timmermann, A., M. Latif, R. Voss, and A. Grötzner, Northern Hemisphere interdecadal variability: A coupled air-sea mode, *J. Clim., 11,* 1906-1931, 1998.

Timmermann, A., J. Oberhuber, A. Bacher, M. Esch, M. Latif, and E. Roeckner, Increased El Niño frequency in a climate model forced by future greenhouse warming, *Nature, 398,* 694-697, 1999.

Ulbrich, U., and M. Christoph, A shift of the NAO and increasing storm track activity over Europe due to anthropogenic greenhouse gas forcing, *Clim. Dyn., 15,* 551-559, 1999.

Voss, R., R. Sausen, and U. Cubasch, Periodically synchronous coupled integrations with the atmosphere-ocean general circulation model ECHAM3/LSG, *Clim. Dyn., 14,* 249-266, 1998.

Wallace, J. M., C. Smith, and C. S. Bretherton, Singular value decomposition of wintertime sea surface temperature and 500-mb height anomalies, *J. Clim., 5,* 561-576, 1992.

H.-F. Graf, J. Perlwitz, and R. Voss, Max-Planck Institute for Meteorology, Bundesstrasse 55, D-20146 Hamburg, Germany. (e-mail: graf@dkrz.de; judith.perlwitz@dkrz.de; reinhard.voss@dkrz.de)

Received April 15, 1999; revised October 22, 1999; accepted November 2, 1999.

This preprint was prepared with AGU's LaTeX macros v5.01. File cctex3 formatted December 7, 1999.

Table 1. Zonal Mean Zonal Component of the Geostrophic Wind (u_g) and Amplitude (A_k) of Waves of Zonal Wave Numbers (ZWNs) $k = 1$ and $k = 2$ for the Heterogeneous Regression Patterns of 50- and 500-hPa Geopotential Heights at 58°N

	50 hPa		500 hPa	
	Weak PVR*	Strong PVR	Weak PVR	Strong PVR
u_g, m/s	2.1	1.2	1.0	0.8
A_1, gpm	24 (96%)	34 (66%)	9 (89%)	8 (30%)
A_2, gpm	3 (1%)	24 (32%)	1 (1%)	11 (58%)

The explained fractions of latitudinal variance of ZWNs 1 and 2 are given in parentheses.

*PVR, polar vortex regime

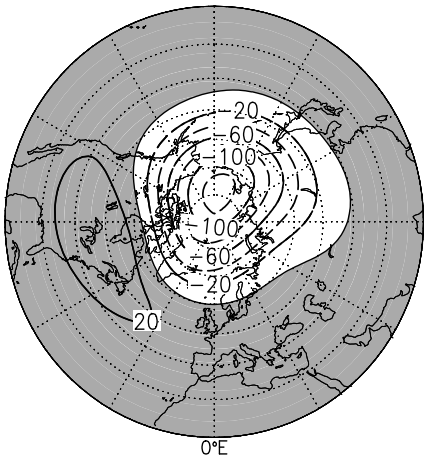

Figure 1. Winter mean Northern Hemisphere (NH) 50-hPa geopotential heights regressed onto temporal expansion coefficients of the 50-hPa singular pattern of the leading atmospheric circulation mode, determined from singular valid decomposition (SVD) analysis between the time series of the 50- and 500-hPa geopotential height field. Contour interval is 20 geopotential meters (gpm). Positive values are shaded.

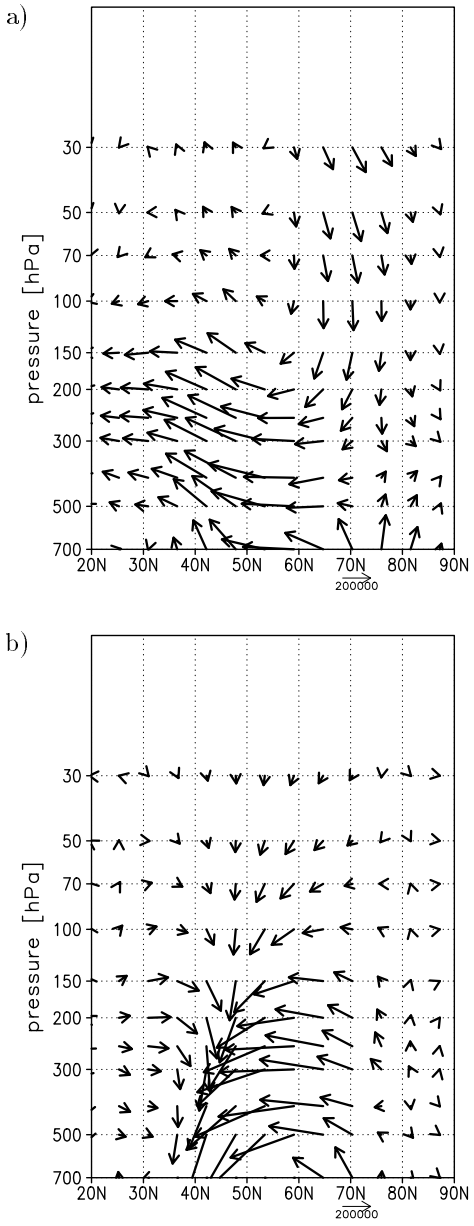

Figure 2. Meridional cross section of difference vectors between the composites of the Eliassen-Palm (E-P) flux (strong minus weak polar vortex state) for (a) zonal wave number (ZWN)1 and (b) ZWN2. The arrow scale amounts to 2.0×10^5 kgs^{-1}. The vertical scaling factor c is 125.

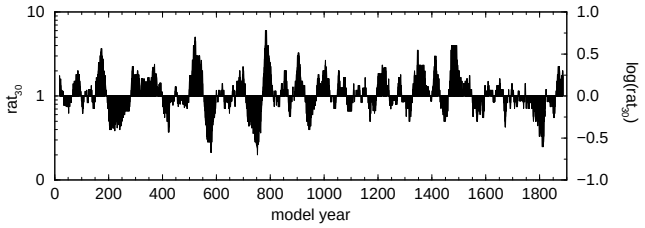

Figure 3. Time series of the ratio of numbers of positive to negative enhancement of the strength of the stratospheric polar vortex for overlapping 30-year periods as described in text.

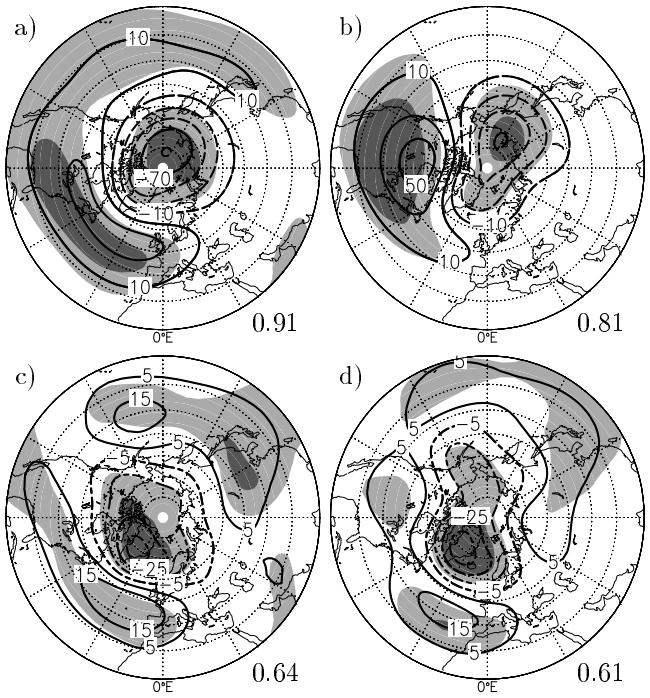

Figure 4. Regression patterns of SVD analysis between the time series of 50- and 500-hPa geopotential heights for the weak and strong polar vortex regimes (PVRs): (a) 50 hPa, weak PVR, (b) 50 hPa, strong PVR, (c) 500 hPa, weak PVR, and (d) 500 hPa, strong PVR. The contour intervals are 20 gpm (50-hPa maps) and 10 gpm (500-hPa maps). The light (dark) shading indicates that the absolute correlation coefficients between the time series of the expansion coefficients and of the local geopotential heights exceeds 0.3 (0.5). The numbers in the bottom right corner of each panel indicate the pattern correlation coefficients between the regression patterns of the model and observations.

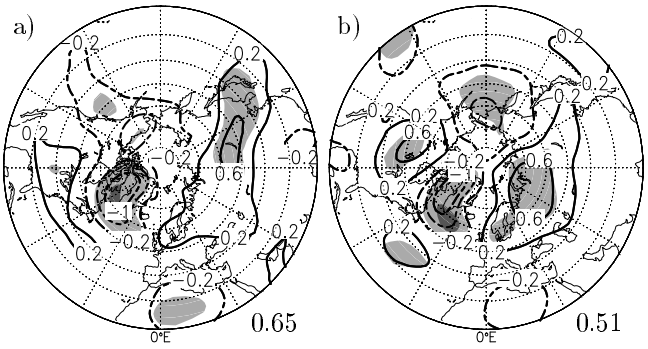

Figure 5. The 850-hPa temperature regressed on the temporal expansion coefficient of the 50-hPa singular pattern for the (a) weak and (b) strong PVR. The contour interval is 0.4 K. The light (dark) shading indicates that the absolute correlation coefficients between the time series of the expansion coefficients and of the local temperature exceeds 0.3 (0.5).

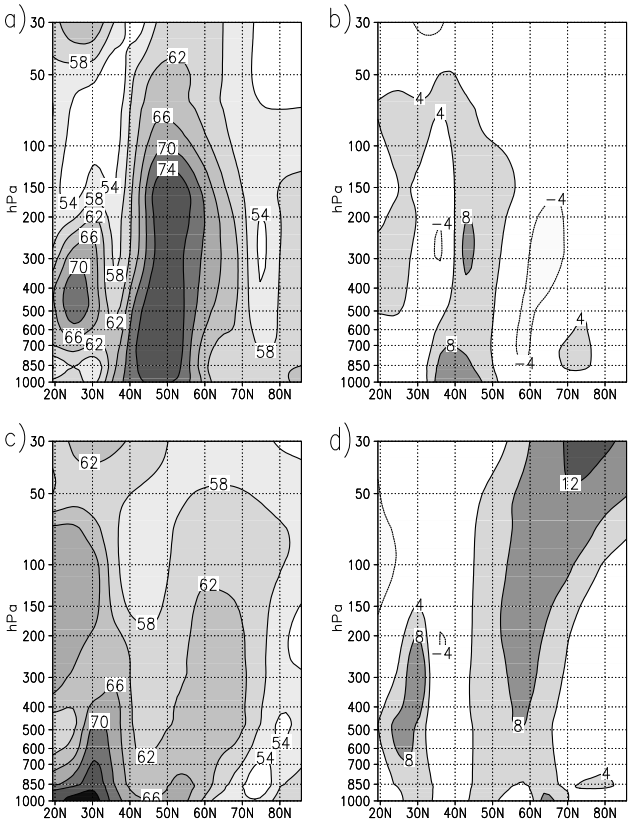

Figure 6. Meridional cross section of the explained fraction of total variance of the leading empirical orthogonal function (percent) as described in text. Shown are (a) weak PVR, ZWN1; (b) strong minus weak PVR, ZWN1; (c) weak PVR, ZWN2; and (d) strong minus weak PVR, ZWN2.

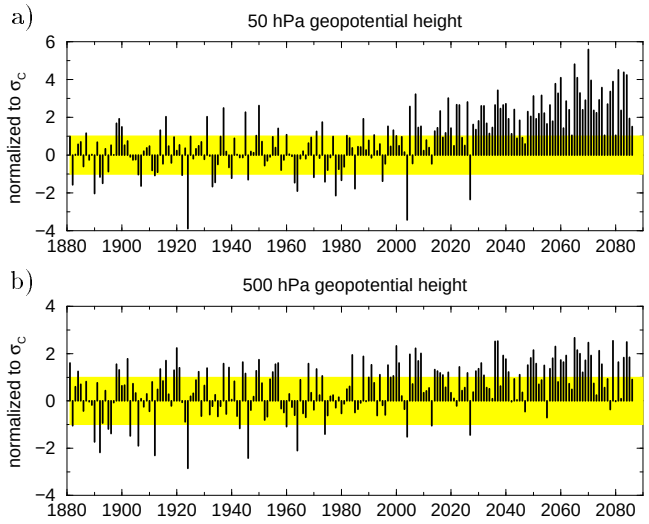

Figure 7. Time series of projections of response pattern, determined from a transient greenhouse gas (GHG) forcing experiment, onto the singular patterns of leading atmospheric circulation mode, determined from the 1900-year control run. The time series for (a) 50-hPa geopotential height field (north of 20°N) and (b) 500-hPa geopotential height field (north of 20°N) are nomalized by the standard deviation σ_C of the individual projections of the control run.

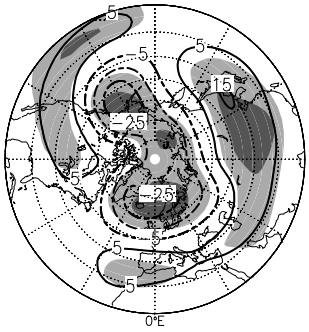

Figure 8. The 500-hPa heterogeneous regression patterns of SVD analysis between 50- and 500-hPa geopotential heights for the GHG experiment on the basis of the time period 2014–2084 of the simulation. The shading corresponds to Figure 4.

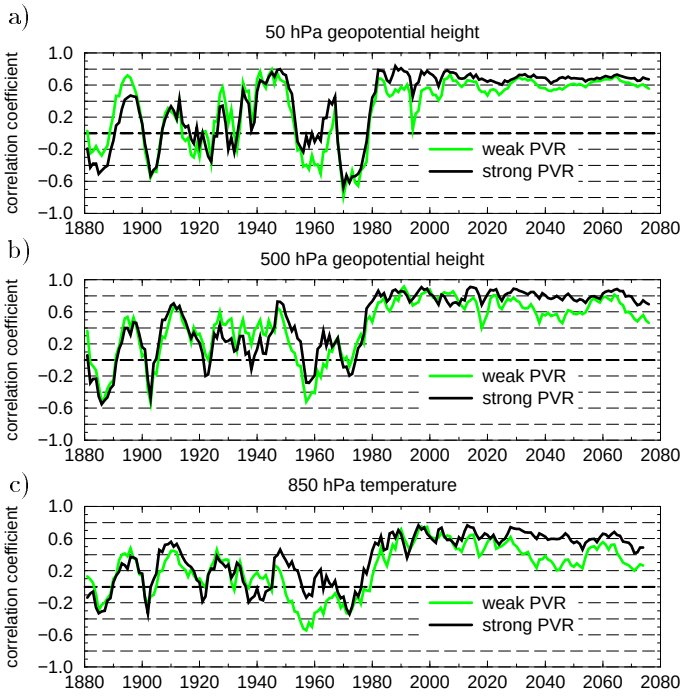

Figure 9. Time series of the spatial pattern correlation between the decadal response patterns and the singular patterns of the model's leading coupled circulation mode for both the model's weak PVR (solid line) and strong PVR (shaded line). Shown are (a) 50-hPa geopotential height field (north of 20°N), (b) 500-hPa geopotential height field (north of 20°N), and (c) 850-hPa temperature (north of 20°N). The corresponding reference patterns of the 850-hPa temperature are given in Figure 5.